IET Image Processing

Research Article

IET Journals
The Institution of Engineering and Technology

GrabCut algorithm for dental X-ray images based on full threshold segmentation

ISSN 1751-9659
Received on 22nd December 2017
Revised 21st June 2018
Accepted on 13th September 2018
E-First on 11th October 2018
doi: 10.1049/iet-ipr.2018.5730
www.ietdl.org

Jiafa Mao[1], Kaihui Wang[1] ✉, Yahong Hu[1], Weiguo Sheng[2], Qixin Feng[3,4]

[1]*College of Computer Science and Technology, Zhejiang University of Technology, Hangzhou, Zhejiang 310023, People's Republic of China*
[2]*Department. of Computer Science, Hangzhou Normal University, Hangzhou 311121, People's Republic of China*
[3]*Xinjiang Institute of Ecology and Geography, Chinese Academy of Sciences, Urumqi 830011, Xinjiang, People's Republic of China*
[4]*University of Chinese Academy of Sciences, Beijing 100049, People's Republic of China*
✉ *E-mail: 1210997496@qq.com*

Abstract: Teeth are difficult to be destroyed due to their corrosion resistance, high melting point and hardness. Dental biometrics can therefore provide assistance in human forensic identification, especially to the unknown corpses. One of the key issue in dental based human identification is the segmentation of Dental X-ray images. In this paper, a novel segmentation algorithm has been proposed for this purpose. The proposed algorithm is based on full threshold segmentation. We first obtain the outline image set $Iwhole_n$ and crown image set $Icrown_m$ of the complete target tooth. Morphological open operation is then applied to the difference images of $Iwhole_n$ and $Icrown_m$. Subsequently, the most complete target tooth image and its corresponding crown image are selected. Getting independent target tooth image I_{contour} and its crown image I_{crown} from these two images. Median filtering is applied to the synthetic image of I_{contour} and I_{crown}, and the resulted image will be used as the Mask for GrabCut to obtain the target tooth image. Experimental results show our proposed algorithm can effectively overcome the problems of uneven grayscale distribution and adhesion of adjacent crowns in dental X-ray images. It can also achieve a high segmentation accuracy and outperform related methods to be compared.

1 Introduction

1.1 Motivation

Unknown corpses usually need to be identified [1, 2] after certain disasters such as earthquake, mudslide, fire and crime scenes. Such corpses are typically difficult to be identified since they lack facial, fingerprint, and other import biological features. DNA detection technology [3] could be helpful in this case, however, it is costly and time-consuming, render their applications. As one of the biological features of the human body, the tooth has the characteristics of the high melting point, strong corrosion resistance, high anti-degradability and hardness [4]. It can be served as a good feature for identification purpose. With the development of the digitalisation of stomatology images and the advancement of computer image processing technology, the identification of individual identities using dental X-ray images [5, 6, 7, 8, 9] has drawn much attention. It has now become one of the hot research topics for human identification [10]. To implement identification using dental X-ray images, it is necessary to segment the teeth of interest and obtain their complete contour, and then extract features. Then, the values of these features from different teeth can be stored for identification purpose. In this case, the performance of the identification method greatly depends on the segmentation algorithm used. It is therefore desirable to have an accurate and robust segmentation algorithm to process the dental X-ray images.

1.2 Related work

Dental neck and root are enwrapped by gums, the crowns of adjacent teeth are closely linked and different structures of the teeth have different dental densities [11]. Usually, the boundary between the root and gums are not clear, and the overall greyscale distribution is uneven in dental X-ray images. Overall, the greyscale of the target and background is very similar, which makes the segmentation extremely difficult.

In [12, 13, 14], researchers employ iterative thresholds on dental radiographs and then performed adaptive threshold segmentation to separate the teeth from the background and tooth-bone regions. After that, the horizontal integral projection and the vertical integral projection are used to separate each individual tooth.

In [15, 16], the dental X-ray images are firstly enhanced to separate the gums from the teeth, then Canny edge detection is applied to the enhanced image to detect all edges and broaden the edges through morphological dilation. Subsequently, a horizontal projection and a vertical projection are applied to a binary image, dividing it into regions of interest so that each image contains one tooth. Finally, the Canny edge operator is performed to each region of interest, and the contour of each tooth is obtained by performing equal points sampling and B-spline fitting.

Wanat and Frejlichowski presented a segmentation algorithm for dental X-ray images in [17]. It first determines the jaws gaps line which is the separation line of upper and lower jaw by choosing the horizontal integral projection with the lowest value that is also close to the centre of the image. Then use the curve to estimate the position of the neck of every tooth and locate the areas between the necks of teeth. After that, the end of teeth is detected by a method. Finally, use the above location information to segment the dental X-ray image into the single tooth.

1.3 Contribution of this paper

In order to appropriately segment and extract dental X-ray target teeth, a novel algorithm has been proposed. The specific contributions of this paper are as follows:

(i) A novel method is proposed based the full threshold segmentation. In this method, we first get the minimum and maximum grey value of the dental X-ray image to be segmented. Iterative threshold operation is then performed, starting with (minimum + 1) and increasing by 1 until maximum. Each threshold operation is performed on the original image. Finally, we obtain an

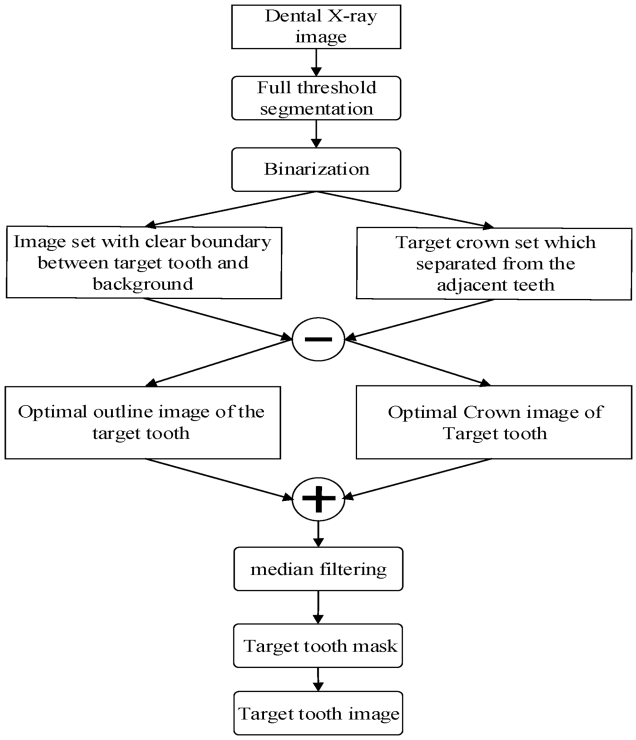

Fig. 1 *Flowchart of the proposed segmentation algorithm*

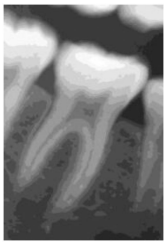

Fig. 2 *Experimental image*

image set, which can reflect the change in the grey level of the original image.

(ii) A new method to obtain the target tooth Mask. In this method, we use the characteristics of different tooth structures with different densities to decompose and synthesise dental X-ray images of different grey levels. The goal is to obtain the Mask image of the target tooth. This method is based on the full threshold segmentation.

(iii) A method to measure the accuracy of the segmentation algorithm. We also compare our method with several related image segmentation algorithms and quantitative analyse the results based on the proposed measure. The results show our algorithm can give a high accurate performance and outperform related methods.

2 Proposed algorithm

To deal with the dental X-ray images, in which greyscale is uneven, adjacent crowns are closely linked, gums are adhesion to the root and low contrast, a novel algorithm has been proposed. In the following sections, the word 'background' refers to a black area in the image, the tooth that will be segmented is called target tooth. The procedure of the proposed algorithm is shown in Fig. 1.

2.1 Full threshold segmentation of dental X-ray images

Our proposed algorithm is based on full threshold segmentation. The image to be segmented is denoted as I_S, and P_{ij} is the grey value at pixel (i, j) in I_S, t represents the threshold. Then, we can define

$$k = t - \min \tag{1}$$

$$T = \{T_k | T_k = \begin{cases} I_S(P_{ij}) & P_{ij} \geq t \\ 0 & P_{ij} < t \end{cases} k = 1, 2, \ldots, (\max - \min); t \in [\min + 1, \max] \tag{2}$$

Here *min* and *max* are the minimum and maximum pixel greyscales, respectively, in the image to be segmented, and $t = \min + 1$ is the initial segmentation threshold, $t = \max$ is the termination segmentation threshold. All the pixels in the image I_S with the grayscale value P_{ij} less than the threshold t are reset to 0. Iterative run threshold segmentation for (max–min) times and each threshold segmentation process is performed on the original image I_S. Then the full threshold segmentation image set T_k of I_S can be obtained. For each segmentation result, we mark it as k, where $k = t - \min$. Fig. 2 show the experimental image used in this paper, and Figs. 3*a* and *b* are partial images obtained from the full threshold segmentation set T_k.

2.2 Target tooth mask obtainment

From Figs. 3*a* and *b*, it is clear that the grey value of the tooth root area is relatively low while the grey value of the crown area is high. From Fig. 3*a*, we can also find that as the threshold increases, the boundary between the target tooth and background gradually becomes clear, and the pulp and gums slowly become the background area. When $k > 84$ (i.e. the segmentation threshold $t > = 84 + \min$), the root gradually loses its complete shape. In Fig. 3*b*, when the segmentation threshold $t = 121 + \min$, the crown of the target tooth is just separated from the adjacent tooth, and as the threshold increases, the crown of the tooth is also gradually reduced. The two tooth images completely marked with a red box in Figs. 3*a* and *b* are extracted separately, as shown in Figs. 4*a* and *b*.

In Fig. 4*a* $k = 78$ (i.e. threshold $t = 78 + \min$), although the outline of the target tooth is not independent but clearly visible. In Fig. 4*b*, the crown of the target tooth is just separated from the adjacent tooth while the root part is blurred.

Then binarisation is performed on the images in T_k. In order to obtain an accurate segmentation result, comparative analysis of image set has been employed. Choose an image with a clear boundary between the target tooth and the background as well as its next six pictures as the target tooth with a complete outline set $Iwhole_n$ $(n = 1, 2, \ldots, 7)$ from the binarised T_k set. Choose an image that the crown is separated from its adjacent teeth and its next six pictures as the complete crown of the target tooth set $Icrown_m (m = 1, 2, \ldots, 7)$ from the binarised T_k set. Each image in $Iwhole_n$ subtracts the corresponding image in $Icrown_m$. During the difference operation, the result images will be automatically numbered as $(Id_{w_i} - Id_{c_j})$contour. Here, Id_{w_i} represents the subscript of each image in $Iwhole_n$ corresponding to binarised T_k and Id_{c_j} denotes the subscript of each image in $Icrown_m$ corresponding to binarised T_k. After the difference operation, some small black spots will appear inside the tooth outline. To remove these noise and smooth the image, the morphological open operation is applied to the results in the previous step.

Fig. 5 is a partial result image after executing the algorithm. Each result in the figure is very similar, so we compared them to the target tooth profile area that segmented by hand. The best one is chosen as the outline of the target tooth. In this paper, we choose the image shown in the red box in Fig. 5. We can get that image by applying a morphological open operation after difference operation of the binary images of Figs. 4*a* and *b*. The specific process is shown in Fig. 6.

The GrabCut algorithm is carried out to obtain a picture that only has the outline of a target tooth from the result of Fig. 6, marked as I_{contour}. The GrabCut algorithm is also used to obtain the corresponding crown picture of I_{contour}, marked as I_{crown}. The resulting I_{contour} and I_{crown} are showing in Figs. 7*a* and *b*.

Next, as shown in Fig. 8, we add I_{contour} and I_{crown} to get the basic shape of the target tooth Mask. During this process, if the

a

b

Fig. 3 *Part images from full threshold segmentation set*
(a) Subfigure 1, ***(b)*** Subfigure 2

sum of two pixels is greater than 1, set the value to 1. To eliminate black noise and retain the edge details, median filtering is applied to the Mask. Finally, the complete Mask image of the target tooth I_{mask} is obtained, as shown in Fig. 9.

2.3 Target tooth image obtainment via grabCut

Graph Cut [18] algorithm maps an image with n pixels into a network with $n+2$ nodes. This network graph is represented as an undirected graph $G=(V, E)$, where V is a finite set of non-empty nodes and E is an edge set of a disordered node pair. The two new nodes are the source point S and sink point T, which represent the convergence point of the target pixel and the background pixel,

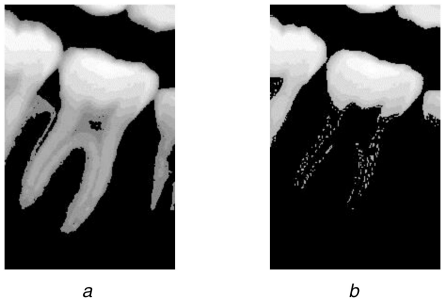

a *b*

Fig. 4 *Two tooth images completely marked with a red box in Fig. 3*
(a) Clear outline of target tooth and ***(b)*** Complete crown

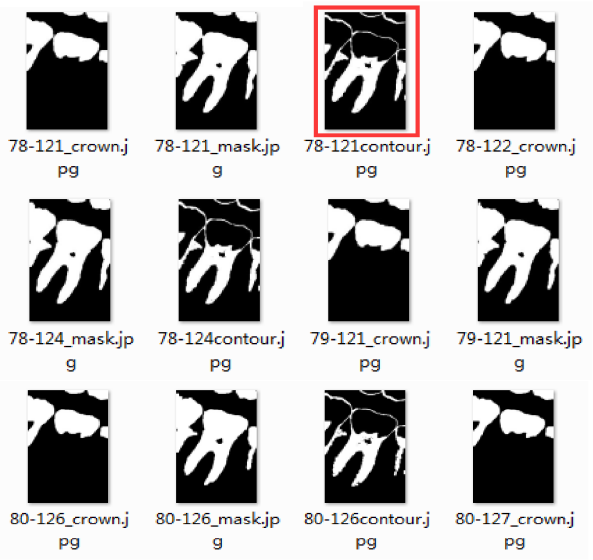

Fig. 5 *Part images of the difference operation*

Fig. 6 *Subtraction operation demonstration*

respectively. In addition to the interconnection between pixels in the image, all target nodes are connected to the source point S, and all background nodes are connected to the sink point T. And $\beta = V - \{S, T\} = \{\beta_1, \beta_2, \ldots, \beta_n, \ldots, \beta_N\}$, $\beta_n \in \{0, 1\}$, which is a vector representing the value of each pixel, the background area marked as 0, the target area marked as 1, as shown in Figs. 10*a* and *b*. Finally, the network model is cut to obtain the minimum cut of the network model, i.e. the minimum value of the energy function, so as to obtain the segmentation result as shown in Figs. 10*c* and *d*.

The GrabCut algorithm is an improved version of Graph Cuts [19]. GrabCut uses the texture and boundary information in the image as the segmentation basis, reducing the amount of user interaction. The image in RGB colour space also works, because it uses a Gaussian mixture model (GMM) instead of the histogram to describe the distribution of foreground and background pixels. The foreground and background areas each correspond to a full-covariance GMM, which consists of K components (generally $K=5$). To facilitate the implementation of GMM, a new vector $\boldsymbol{k} = \{k_1, k_2, \ldots, k_n, \ldots, k_N\}$ is introduced and $k_n \in \{1, \ldots, K\}$ represents the Gauss component corresponding to the nth pixel. Each pixel belongs to the foreground or backgrounds GMM totally up to $\beta_n \in (0, 1)$, so the segmentation of image can be done through marking the image pixels, and the optimal segmentation of the

Fig. 7 *Initial results of the application of GrabCut*
(a) Demonstration of I_{contour}, ***(b)*** Demonstration of I_{crown}

Fig. 8 *Demonstration of* $I_{contour}+I_{crown}$

Fig. 9 *Mask of the target tooth*

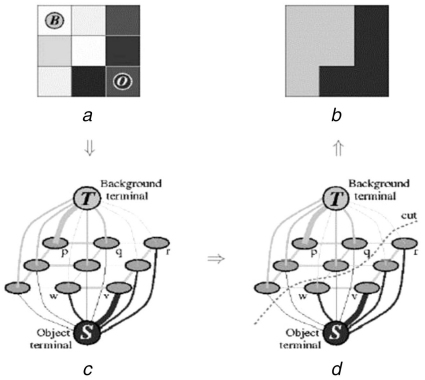

Fig. 10 *Segment principle of Graph Cut [18]*

Fig. 11 *Image of the target tooth*

image is to find the best pixel label. Researchers have deduced that the max flow of the network is the min cut. Therefore, the entire segmentation process can be achieved by minimising the energy function. By iterative GMM to solve the energy function minimisation mode effectively improve the segmentation accuracy.

The Gibbs energy used for segmentation is

$$E(\underline{\beta}, k, \underline{\theta}, z) = U(\underline{\beta}, k, \underline{\theta}, z) + V(\underline{\beta}, z) \tag{3}$$

The first part of energy function U is data term

$$U(\underline{\beta}, k, \underline{\theta}, z) = \sum_n D(\beta_n, k_n, \underline{\theta}, z_n) \tag{4}$$

$$D(\beta_n, k_n, \underline{\theta}, z_n) = -\log p(z_n|\beta_n, k_n, \underline{\theta}) - \log \pi(\beta_n, k_n) \tag{5}$$

$p(\cdot)$ is a Gaussian probability distribution, and $\pi(\cdot)$ indicates the mixing weight coefficient, so

$$D(\beta_n, k_n, \underline{\theta}, z_n) = -\log \pi(\beta_n, k_n) + \frac{1}{2}\log \det \sum(\beta_n, k_n) + \frac{1}{2}[z_n - \mu(\beta_n, k_n)]^{\mathrm{T}} \sum(\beta_n, k_n)^{-1}[z_n - \mu(\beta_n, k_n)] \tag{6}$$

$\underline{\theta}$ is the parameter of the GMM

$$\underline{\theta} = \{\pi(\beta, k), \mu(\beta, k), \sum(\beta, k), \beta = \{0, 1\}, k = \{1, 2, \ldots, K\}\} \tag{7}$$

Here $\pi(\beta, k)$, $\mu(\beta, k)$ and $\sum(\beta, k)$ represent the proportion of each Gaussian probability distribution, mean and covariance. The second part of energy function V is a smooth term

$$V(\underline{\beta}, z) = \gamma \sum_{(m,n) \in C} [\beta_n \neq \beta_m] \exp - \alpha z_m - z_n^2 \tag{8}$$

Here C denotes all pairs of adjacent pixels, the greater the difference between adjacent pixels, the smaller the energy between them.

There are two ways for GrabCut to make sure the foreground and background, (i) manually interact with users and (ii) through the mask. The second method can reduce the number of iterations and improve its efficiency. Fig. 11 shows the target tooth image using GrabCut with the mask shown in Fig. 9. The experiments also show that using GrabCut with a mask to segmentation the target tooth image almost requires only one iteration.

3 Experimental results and comparative analysis

3.1 Experiment preparation

The above described method was tested on the database of 244 X-dental images, each sized 1000*800 pixels. And all the experimental images are from the dental clinic of the First Affiliated Hospital of Zhejiang University. The experiments are implemented on a computer with 2.60 GHz CPU and 4 GB memory running the Windows7 64-bit system. Experimental software development platform is Opencv3 and Python3.

Due to the original dental X-ray images are based on IMG format, we transformed them to JPG or PNG format, which the Opencv3 can process. However, the brightness and contrast of images after transformation could seriously affect the results of our proposed algorithm, so we unified all the dental X-ray images contrast and brightness, they were 20,19.

3.2 Comparative analysis

Experiment 1: We compared our algorithm with improved C-V level set algorithm proposed by Li *et al.* [20], GrabCut algorithm [19] and Morph–Snakes algorithm [21]. Fig. 12 shows the process of obtaining the target image by directly applying GrabCut. As shown in Fig. 12*a*, it needs to draw a rectangle in dental X-ray image to make sure the foreground and the background first. Then iterative the GMM to obtain the minimum cut of the energy function. Because of the characteristic of the dental X-ray image, it cannot segment any area after a few iterations. Only by manually marking the foreground and background many times we can get the

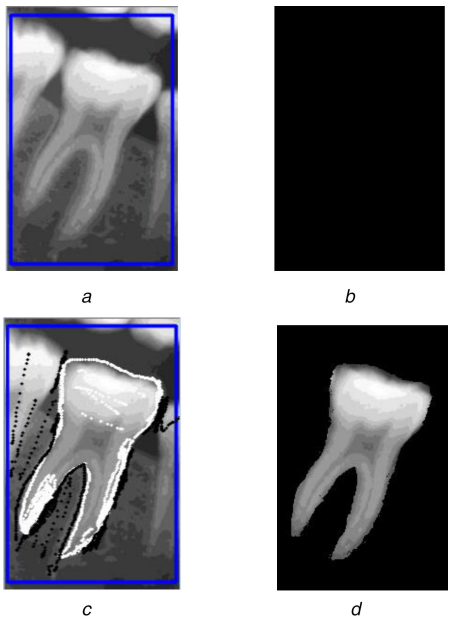

Fig. 12 *Process of GrabCut segmentation of dental X-ray image*
(a) Image with a rectangle to make sure the foreground and background, ***(b)*** Image after several GMM iterations, ***(c)*** Image of marking the foreground and background by hand, ***(d)*** The target image obtained by GrabCut

Fig. 13 *Result of the C-V level set segmentation in [20]*

Fig. 14 *Result of Morph-Snakes segmentation in [21]*

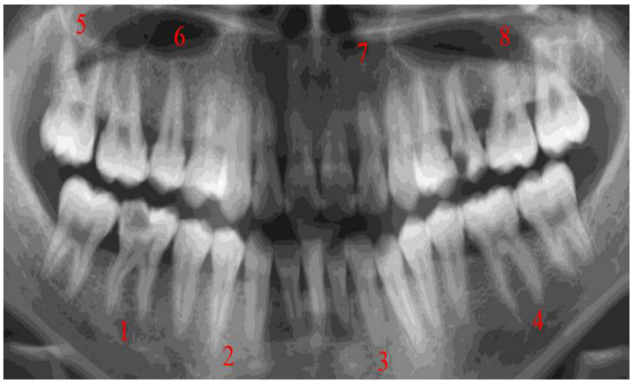

Fig. 15 *Full X-ray Dental image*

result shown in Fig. 12*d*. Comparing the results obtained by directly applying GrabCut and our proposed algorithm, the shape of the crown segment by our algorithm is more complete, and the separation of the root and the gum is more thorough. Moreover, the segmentation result of the GrabCut algorithm is affected by hand, so the result is unstable.

Fig. 13 shows the result of C-V level set segmentation in [20]. Although the initial contour is set, it still cannot overcome the problem of adjacent tooth crowns being closely connected during curve evolution. So that the segmentation result includes adjacent teeth. If you set this contour as the Mask for GrabCut, its segmentation process is the same as using GrabCut directly, you need to manually mark the foreground and background multiple times. Fig. 14 is the result of Morph–Snakes segmentation algorithm after 240 iterations. It is clear that the segmentation contour is smaller than the contour of the actual target tooth. Compared with the above segmentation algorithms, the proposed algorithm in this paper can effectively overcome the problems of the crown between adjacent teeth, which is closely connected and the uneven greyscale distribution of dental X-ray images. And the segmentation process is fast and easy to implement.

Experiment 2: In order to quantitatively analyse [22] the accuracy of the segmentation algorithms, the proposed algorithm, GrabCut algorithm and Morph–Snakes algorithm were applied to eight tooth images marked with a red number in Fig. 15. Definition the area of target teeth segmented by the above algorithms is S_{med}, and by hand is S_{hand}. The operator Δ_{Dev} used to measure the accuracy is defined as

$$\Delta_{\text{Dev}} = \frac{\left|\left(S_{\text{med}} \cup^{S}_{\text{hand}}\right) - \left(S_{\text{med}} \cap^{S}_{\text{hand}}\right)\right|}{S_{\text{hand}}} \tag{9}$$

Smaller Δ_{Dev} indicates the higher accuracy of the algorithm. Fig. 16 shows the segmentation results of the above algorithms. The first row shows eight original dental X-ray images for comparison experiment, the second row is the result of manual segmentation, the third row is the result by our proposed segmentation algorithm, the fourth row is the result of GrabCut segmentation algorithm, the fifth line is the result of the Morph–Snakes segmentation algorithm.

The specific segmentation results are shown in Table 1. For those eight dental X-ray images, it is clear that the deviation of Morph–Snakes algorithm is higher than the other two algorithms. The deviation of the algorithm proposed in this paper is mostly <0.2 and relatively low, which means the segmentation accuracy is higher than related methods. From the average deviation, the GrabCut algorithm is 0.2013, Morph–Snake algorithm is 0.4467, and our proposed algorithm gives 0.1489. The average deviation of our algorithm is one-third of Morph–Snakes and seven in ten of GrabCut. Therefore, for dental X-ray images, the proposed algorithm in this paper can get more accurate segmentation results. From the table, we can see that the deviation of **pic3** and **pic7** is slightly higher than other images in the fourth column. This is because the grey values of the crow and root are not changed much in those two pictures. During the full threshold segmentation, the roots did not completely disappear when the threshold was increased to a certain extent. That leads to the mask may not be complete. Although the results are not very bad, we still have to find a solution to this problem in our future work.

We randomly selected 50 individual tooth X-ray images from the database and segmented by applying the above mentioned segmentation algorithms. The resulting deviation is shown in Fig. 17. The X-axis represents 50 dental X-ray images, and the *y*-axis represents deviation. The dashed lines of different colours in the figure indicate the average of deviations generated by different segmentation algorithms. It can be seen from the figure that the segmentation result is similar to the previous eight images. Thus, our proposed segmentation method still has a high accuracy rate.

4 Conclusions

Dental X-ray images are suffered from uneven distribution of greyscale and the crown of adjacent teeth tightly connected, which makes the task of segmentation extremely difficult. In order to

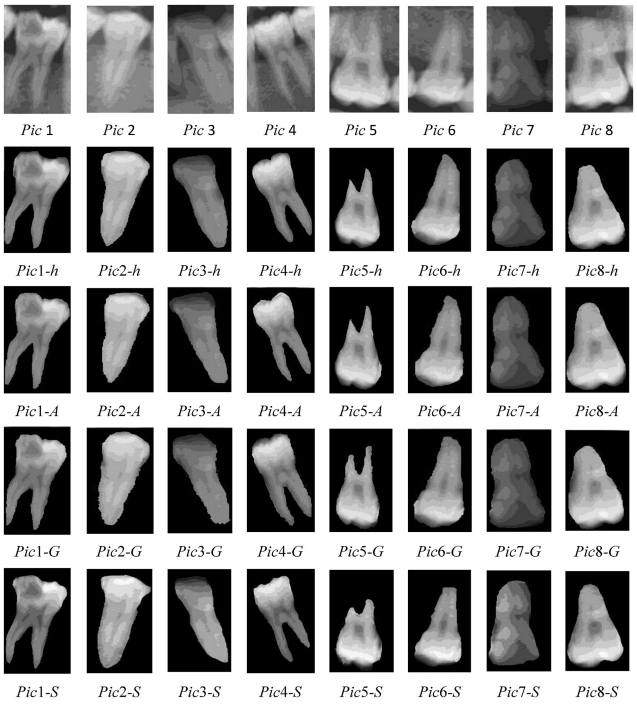

Fig. 16 *Image of experimental comparison*

Table 1 Quantitative analysis and comparison of different segmentation algorithms for eight dental X-ray images

Dental X-ray images	Deviation of GrabCut	Deviation of Morph–Snakes	Deviation of the algorithm in this paper
Pic1	0.1696	0.4198	0.1026
Pic2	0.2143	0.4867	0.1338
Pic3	0.2307	0.4096	0.2087
Pic4	0.1320	0.3074	0.0673
Pic5	0.1004	0.3980	0.0652
Pic6	0.2128	0.4306	0.1779
Pic7	0.2925	0.5687	0.2812
Pic8	0.2581	0.5527	0.1549
average deviation	0.2013	0.4467	0.1489

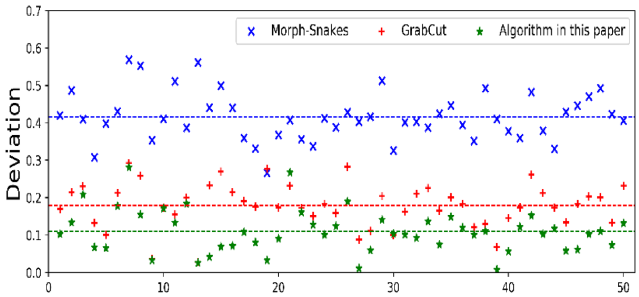

Fig. 17 *Image of deviation distribution of the above segmentation algorithms*

address such a problem, a GrabCut algorithm for dental X-ray images based on full threshold segmentation is proposed in this work. Thanks to the grey problem of dental X-ray images, we presented a full threshold segmentation method. By fully usage of different tooth structures in dental X-ray images with different greyscale, the complete shape and crown image of the target tooth can be obtained from the full threshold segmentation set. The difference and the synthesis operation are performed on them to obtain the Mask image of the target tooth. Finally, GrabCut is applied to the Mask to obtain the target tooth image. Experimental results show that the proposed algorithm can achieve satisfactory results for the segmentation of dental X-ray images.

5 Acknowledgment

This work is supported by the National Natural Science Foundation of China (Nos. 61573316, 61873082), the National Key R&D Program of China (No. 2018YFB0204003).

6 References

[1] Higgins, D., Austin, J.J.: 'Teeth as a source of DNA for forensic identification of human remains: a review', *Sci. Justice*, 2013, **53**, (4), pp. 433–441

[2] Numata, N., Makinae, H., Yoshida, W., *et al.*: 'Disaster victim identification using orthopedic implants in the 2011 east-Japan earthquake and tsunami', *Tohoku J. Exp. Med.*, 2017, **241**, (3), pp. 219–223

[3] Ziętkiewicz, E., Witt, M., Daca, P., *et al.*: 'Current genetic methodologies in the identification of disaster victims and in forensic analysis', *J. Appl. Genetics*, 2012, **53**, (1), pp. 41–60

[4] Qun, H.: 'Application of dental morphological images in major catastrophic cases', *Imaging Mater.*, 2003, **4**, pp. 13–15

[5] Pushparaj, V., Gurunathan, U., Arumugam, B.: 'Dental radiographs and photographs in human forensic identification', *Iet Biometrics*, 2013, **2**, (2), pp. 56–63

[6] Silva, R.F., Franco, A., Picoli, F.F., *et al.*: 'Dental human identification using bitewing radiographs – a case report', *Eur. J. Forensic Sci.*, 2016, **3**, (3), pp. 31–33

[7] Nomir, O., Abdel-Mottaleb, M.: 'Human identification using individual dental radiograph records', *Case Stud. Intell. Comput. Achievements Trends*, 2014, p. 329

[8] Berketa, J.W., James, H., Lake, A.W.: 'Forensic odontology involvement in disaster victim identification', *Forensic Sci., Med. Pathol.*, 2012, **8**, (2), pp. 148–156

[9] Dighe, S., Shriram, R.: 'Preprocessing, segmentation and matching of dental radiographs used in dental biometrics', Rehili, 2012

[10] Khandare, K.P., Gurjar, A.A.: 'Dental biometric approach for human identification using dental X-ray images of maxillary bone', *Int. Res. J. Eng. Technol.*, 2016, **3**, pp. 1566–1570

[11] Nomir, O., Abdel-Mottaleb, M.: 'Human identification from dental X-ray images based on the shape and appearance of the teeth', *IEEE Trans. Inf. Forensics Sec.*, 2007, **2**, pp. 188–197

[12] Nomir, O., Abdel-Mottaleb, M.: 'Fusion of matching algorithms for human identification using dental X-ray radiographs', *IEEE Trans. Inf. Forensics Secur.*, 2008, **3**, (2), pp. 223–233

[13] Abdel-Mottaleb, M., Nomir, O., Nassar, D.E., *et al.*: 'Challenges of developing an automated dental identification system'. Midwest Symp. on IEEE Circuits and Systems, Cairo, Egypt, 2004, pp. 411–414

[14] Nomir, O., Abdel-Mottaleb, M.: 'A system for human identification from x-ray dental radiographs', *Pattern Recognit.*, 2005, **38**, (8), pp. 1295–1305

[15] Lin, P.L., Lai, Y.H., Huang, P.W.: 'Dental biometrics: human identification based on teeth and dental works in bitewing radiographs', *Pattern Recognit.*, 2012, **45**, (3), pp. 934–946

[16] Lin, P.L., Lai, Y.H., Huang, P.W.: 'An effective classification and numbering system for dental bitewing radiographs using teeth region and contour information', *Pattern Recognit.*, 2010, **43**, (4), pp. 1380–1392

[17] Wanat, R., Frejlichowski, D.: 'A problem of automatic segmentation of digital dental panoramic X-ray images for forensic human identification', Proc. 15th Central European Seminar on Computer Graphics, Viničné, Slovakia, May 2011

[18] Boykov, Y.Y., Jolly, M.P.: 'Interactive graph cuts for optimal boundary & region segmentation of objects in N-D images'. IEEE Int. Conf. Computer Vision IEEE Computer Society, Vancouver, Canada, 2001

[19] Rother, C., Kolmogorov, V., Blake, A.: ''Grabcut': interactive foreground extraction using iterated graph cuts', *ACM Trans. Graph.*, 2004, **23**, (3), pp. 309–314

[20] Li, C., Xu, C., Gui, C., *et al.*: 'Distance regularized level set evolution and its application to image segmentation', *IEEE Trans. Image Process. A Publ. IEEE Signal Process. Soc.*, 2010, **19**, (12), pp. 3243–3254

[21] Álvarez, L., Baumela, L., Henríquez, P., *et al.*: 'Morphological snakes', *Comput. Vis.Pattern Recognit.*, 2010, **26**, pp. 2197–2202

[22] Wu, T., Zhang, L.B.: 'Three dimension tooth reconstruction using level set active contour model', *J. Image Graph.*, 2016, **21**, (8), pp. 1078–1087